Theoretical Analysis and Experimental Study on SO_2 Adsorption onto Pistachio-nut-shell Activated Carbon

Aik Chong Lua and Ting Yang
School of Mechanical and Aerospace Engineering, Nanyang Technological University, 50 Nanyang Avenue, Singapore 639798, Republic of Singapore

DOI 10.1002/aic.11684
Published online December 15, 2008 in Wiley InterScience (www.interscience.wiley.com).

The adsorption study of SO_2 onto the activated carbon prepared from pistachio-nut shell was studied theoretically and experimentally. A single-particle sorption model known as concentration-dependent surface diffusivity micropore, surface and macropore diffusion control model incorporating micropore, macropore and surface diffusions, together with a nonlinear isotherm at the micropore mouth, has been derived and solved by a finite difference method. The effects of different types of nonlinear isotherms and concentration dependent surface diffusivities have been thoroughly studied. The effects of adsorbate concentration and temperature on adsorption were studied experimentally. Good agreement was found between the model predictions and the experimental results. The value of the tortuosity factor and the extracted diffusion coefficients obtained are consistent with their corresponding values reported. © 2008 American Institute of Chemical Engineers *AIChE J,* 55: 423–433, 2009

Keywords: adsorption, sulfur dioxide, isotherm, sorption model, activated carbon, surface diffusivity, finite difference method

Introduction

Important and integral to adsorption calculations and modeling is the prediction or estimation of adsorbate uptake rates by the adsorbent particle. For the transport of adsorbate from the bulk fluid to the interior of a pellet before adsorption takes place, the following mass transfer processes may be present: external and internal diffusions. The internal diffusion can have three different diffusion mechanisms, pore diffusion, surface diffusion and combined pore and surface diffusion.

Numerous workers have attempted to model the sorption process using either single diffusion resistance[1–4] or combined pore diffusion and surface diffusion resistance.[5,6] However, for microporous adsorbent of moderate size, resistance to mass transport is usually significant at both macropore and micropore regions, therefore, a bidispersed model has to be used to describe the adsorption dynamics.[7–10] In addition to the adsorbate transport through the macropore and micropore regions of the activated carbon, it is possible for gases that adsorb significantly to have an additional flux in the sorbed or "surface" phase which is in parallel to the macropore void diffusion mechanism.[11] A discussion of the different surface diffusion mechanisms is given in a review by Kapoor et al.[12] Gray and Do[13,14] developed the models for single-particle sorption, which comprised of micropore, macropore and surface diffusion, together with a nonlinear isotherm at the micropore mouth. One of these models[14] also considered the effects of particle nonisothermality and concentration dependency of the surface diffusivity.

In the work of Gray and Do,[14] the relationship of concentration dependency of the surface diffusivity was based on the model by Higashi et al.[15] This model had been widely used for its simplicity. However, the effects of different concentration-dependent surface diffusivities on the sorption kinetics have not been studied. The effects of different nonlinear isotherms on the overall particle sorption kinetics have

Correspondence concerning this article should be addressed to A. C. Lua at maclua@ntu.edu.sg.

also not been systematically studied. Therefore, in this article, a new model incorporating micropore, macropore and surface diffusions, together with a nonlinear isotherm at the micropore mouth, is presented. The effects of different nonlinear isotherms and concentration-dependent surface diffusivities have been thoroughly studied.

For the numerical solution, a kinetics model comprising of micropore, macropore and surface diffusion with a nonlinear isotherm used by Gray and Do,[9,10,13,14] was solved by the orthogonal collocation technique. The method of orthogonal collocation, although computationally efficient, leads to significant oscillations in the profiles, particularly when changes in concentration are sharp. For example, according to Gray and Do,[9,10,13,14] under certain circumstances, the numerical integration time became large or the problem became insoluble due to the nature of isotherm or the model itself. Therefore, an additional degeneration process using a special technique was needed. In this article, a finite difference method was adopted and results showed that the aforementioned problems associated with the orthogonal collocation technique, could be overcome. SO_2 adsorption onto commercial activated carbons had been studied by Gray and Do,[10,13] and Gray,[16] and diffusivities of micropore, macropore and surface were reported in these studies.

This article reports on the mathematical development of a single-particle sorption model incorporating micropore, macropore and surface diffusions with a nonlinear isotherm, the solving of the sorption model by a finite difference technique, and the comparison between the numerical results and the experimental results on SO_2 adsorption onto the pistachio-nut-shell activated carbon.

Model Description

The assumptions necessary for the formulation of the single-particle dynamics are as follows:

1. The activated carbon sorbent particle is assumed to have a bidispersed pore-size distribution comprising of a microporous solid penetrated throughout by a network of larger interconnected pores (macropores).
2. The carbon particle is composed of many minute microparticles which contain the micropores and can be of various shapes (e.g., slab, cylinder, or sphere). For model simplicity, however, these are usually assumed to be spherical. These two assumptions which are bimodal pore-size distribution and spherical microparticles are commonly used by other authors in the literature.[9,10,13,14]
3. The carbon particle/pellet geometry is arbitrary (e.g., slab, cylinder or sphere).
4. The resistances controlling the sorption dynamics are due to macropore, micropore, and surface diffusion.
5. The macropore and micropore diffusivities are independent of adsorbate concentration, but the surface diffusivity is coverage-dependent.
6. Adsorption on the macropore surface is negligible compared to the total adsorption capacity.
7. Sorption at the pore mouth of the micropore follows an equilibrium isotherm.
8. The system is isothermal.

Using these assumptions and with the symbols defined in the notation, the mass balance equation for the microsphere may be expressed as

$$\frac{\partial q}{\partial t} = \frac{D}{r_\mu^2}\frac{\partial}{\partial r_\mu}\left(r_\mu^2 \frac{\partial q}{\partial r_\mu}\right) \tag{1}$$

The boundary conditions are

$$r_\mu = 0, \quad \frac{\partial q}{\partial r_\mu} = 0 \tag{1a}$$

$$r_\mu = R_\mu, \quad q = q_m \frac{bC}{1+bC} \quad \text{(Langmuir isotherm)} \tag{1b}$$

The mass balance equation for the particle is

$$\varepsilon_m \frac{\partial C}{\partial t} + (1-\varepsilon_m)\frac{\partial \bar{q}}{\partial t} = \varepsilon_m D_p \frac{1}{r^s}\frac{\partial}{\partial r}\left(r^s \frac{\partial C}{\partial r}\right) + (1-\varepsilon_m) D_s(\theta)\frac{1}{r^s}\frac{\partial}{\partial r}\left(r^s \frac{\partial \bar{q}}{\partial r}\right) \tag{2}$$

The boundary conditions are

$$r = 0, \quad \frac{\partial C}{\partial r} = \frac{\partial \bar{q}}{\partial r} = 0 \tag{2a}$$

$$r = R, \quad \varepsilon_m D_p \left.\frac{\partial C}{\partial r}\right|_R + (1-\varepsilon_m) D_s(\theta)\left.\frac{\partial \bar{q}}{\partial r}\right|_R = K_m(C_b - C|_R) \tag{2b}$$

where $\bar{q}$ is the volume average microsphere concentration, and is given by

$$\bar{q} = \frac{4\pi \int_0^{R_\mu} r_\mu^2 q dr_\mu}{4\pi \int_0^{R_\mu} r_\mu^2 dr_\mu} \tag{3}$$

The initial condition for the adsorption cycle is

$$t = 0, \quad C = q = 0, \quad C_b = C_0 \tag{4a}$$

while the initial condition for the desorption cycle is

$$t = 0, \quad C = C_0, \quad q = q_0, \quad C_b = 0 \tag{4b}$$

The equilibrium isotherm at the pore mouth of the micropore is of the Langmuir isotherm form first. The discussion on the different isotherms will be given in greater details later.

The HIO model by Higashi et al.[15] is used to define the coverage dependence of surface diffusivity such that

$$D_s(\theta) = D_{s0}\frac{1}{1-\theta} \tag{5}$$

The nondimensional variables and parameters are defined following, and in the notation.

$$A = \frac{C}{C_0}; \quad A_\mu = \frac{q}{q_0}; \quad \bar{A}_\mu = \frac{\bar{q}}{q_0}; \quad A_b = \frac{C_b}{C_0} \tag{6}$$

$$x = \frac{r}{R}; \quad x_\mu = \frac{r_\mu}{R_\mu} \tag{7}$$

$$\tau = \frac{(\varepsilon_m D_p)t}{\left[\varepsilon_m + (1-\varepsilon_m)\frac{q_0}{C_0}\right]R^2} \tag{8}$$

$$\gamma = \frac{\left[\varepsilon_m + (1-\varepsilon_m)\frac{q_0}{C_0}\right] DR^2}{\left(\varepsilon_m D_p\right) R_\mu^2} \tag{9}$$

$$Bi_m = \frac{K_m R}{\left(\varepsilon_m D_p\right)} \tag{10}$$

$$\sigma_1 = \frac{\varepsilon_m}{\left[\varepsilon_m + (1-\varepsilon_m)\frac{q_0}{C_0}\right]}; \quad \sigma_2 = 1 - \sigma_1 \tag{11}$$

$$\delta = \frac{(1-\varepsilon_m) D_{s0} q_0}{\varepsilon_m D_p C_0} = \frac{\sigma_2 D_{s0}}{\sigma_1 D_p} \tag{12}$$

$$\lambda = bC_0 \tag{13}$$

In nondimensional form, the microsphere mass balance equation (Eq. 1), becomes

$$\frac{\partial A_\mu}{\partial \tau} = \frac{\gamma}{x_\mu^2}\frac{\partial}{\partial x_\mu}\left(x_\mu^2 \frac{\partial A_\mu}{\partial x_\mu}\right) \tag{14}$$

The boundary conditions are

$$x_\mu = 0, \quad \frac{\partial A_\mu}{\partial x_\mu} = 0 \tag{14a}$$

$$x_\mu = 1, \quad A_\mu = \frac{(1+\lambda)A}{(1+\lambda A)} \tag{14b}$$

The nondimensional particle mass balance equation (Eq. 2), becomes

$$\sigma_1 \frac{\partial A}{\partial \tau} + \sigma_2 \frac{\partial \bar{A}_\mu}{\partial \tau} = \frac{1}{x^s}\frac{\partial}{\partial x}\left(x^s \frac{\partial A}{\partial x}\right) + \delta(1+\lambda A)\frac{1}{x^s}\frac{\partial}{\partial x}\left(x^s \frac{\partial \bar{A}_\mu}{\partial x}\right) \tag{15}$$

The boundary conditions are

$$x = 0, \quad \frac{\partial A}{\partial x} = \frac{\partial \bar{A}_\mu}{\partial x} = 0 \tag{15a}$$

$$x = 1, \quad \left.\frac{\partial A}{\partial x}\right|_1 + \delta\left(1 + A|_1\right)\left.\frac{\partial \bar{A}_\mu}{\partial x}\right|_1 = Bi\left(A_b - A|_1\right) \tag{15b}$$

For the adsorption cycle, the initial conditions are

$$\tau = 0, \quad A = A_\mu = 0; \quad A_b = 1 \tag{16a}$$

For the desorption cycle, the initial conditions are

$$\tau = 0, \quad A = A_\mu = 1, \quad A_b = 0 \tag{16b}$$

where

$$\bar{A}_\mu = 3\int_0^1 x_\mu^2 A_\mu dx_\mu \tag{17}$$

Based on the assumptions of the general adsorption kinetic model, the sorption at the pore mouth of the micropore follows an equilibrium isotherm, and the isotherm should be nonlinear to better describe the model. Normally, the isotherm is of the form of either Langmuir,[14,17] Freundlich,[9,2] Fritz-Schlűnder[4] or Radke-Prausnitz.[3,18] Although the adsorption equilibrium data were fitted with several well-known isotherm models,[4,19] it involved the study of equilibrium property only. So far, there has not been a systematic study of the effect of isotherm type on the adsorption kinetics except for just a preliminary study.[13] Therefore, in this article, emphasis was given to this effect of isotherm type.

Several well-known isotherms used to describe the sorption equilibrium between the adsorbed phase and the free adsorbate phase at the pore mouth of the micropore are shown in Table 1. For the isotherms given in Table 1, there are three parameters, q_m, b and n, which are required in the Sips, R-P, and Toth isotherms, while there are two parameters required in the Langmuir or Freundlich isotherms, which are q_m and b or K and n, respectively.

To use the kinetic model in this study, the nondimensional Langmuir Isotherm (Eq. 14b) is substituted by the different nondimensional isotherms, i.e., Eqs. 31, 33, 34 or Eq. 36 in Table 1, to study the effect of each isotherm type on the adsorption kinetics.

In porous materials, surface diffusion is known to contribute to internal mass transfer. For many adsorption processes, this type of transport is the rate-determining step. Several studies have proven a strong dependence of surface diffusivity on the concentration in the adsorbed phase.[5,20] However, in many investigations on adsorption kinetics and dynamics, for the sake of simplicity[21,13,8] or the lack of information about its concentration dependence, surface diffusivity was taken as a constant.

Some researchers had considered the concentration-dependent surface diffusion.[22,14] The surface diffusivity was taken as a function of the local adsorbate concentration and described by the HIO model[15]

$$D_s(\theta) = D_{s0}\frac{1}{1-\theta} \tag{5}$$

The HIO model is based on a random transport of molecules from one adsorption site to another adsorption site on the solid surface. Another model for surface diffusion in heterogeneous activated carbon is given by Do.[23] In terms of the concentration dependence, the Do model shows a very strong dependence of the surface diffusivity on the adsorbed concentration. The dependence of D_s on fractional loading takes the following form

$$\frac{D_s}{D_{s0}} = \frac{1}{(1-\theta)^2} \tag{18}$$

Although Eq.18 is obtained from the actual conditions such as a specific isotherm, it can still be used as another equation in the kinetic model to describe the concentration-dependent surface diffusivity for it exhibits a much stronger dependence on the concentration than the traditional HIO model.

Two models, namely HIO model (Eq. 5), and Do model (Eq. 18), are used to describe the concentration-dependent surface diffusivity. To solve the kinetic model using the Do model, the HIO model is substituted by the Do model in Eq. 2 so that the effects of different concentration-dependent surface diffusivity type on the adsorption kinetics can be studied.

Table 1. Commonly Used Isotherm Expressions

Isotherm model	Expression		Non-dimensional Expression	
1) Langmuir	$q = q_m \frac{bC}{1+bC}$	(1b)	$A_\mu = \frac{A(1+\lambda)}{(1+\lambda A)}$	(14b)
			$\lambda = bC_0$	(13)
2) Langmuir-Freundlich (or Sips)	$q = q_m \frac{bC^n}{1+bC^n}$	(27)	$A_\mu = \frac{A^n(1+\lambda)}{(1+\lambda A^n)}$	(31)
			$\lambda = bC_0^n$	(32)
3) Freundlich	$q = KC^{1/n}$	(28)	$A_\mu = A^{1/n}$	(33)
4) Rudke-Prausnitz (or R-P)	$q = q_m \frac{bC}{1+bC^n}$	(29)	$A_\mu = \frac{A(1+\lambda)}{(1+\lambda A^n)}$	(34)
			$\lambda = bC_0^n$	(35)
5) Toth	$q = q_m \frac{b^{1/n}C}{(1+bC^n)^{1/n}}$	(30)	$A_\mu = \frac{A(1+\lambda)^{1/n}}{(1+\lambda A^n)^{1/n}}$	(36)
			$\lambda = bC_0^n$	(37)

Method and Procedure of Numerical Solution

The equations in the model are nonlinear partial differential equations, and, therefore, the solutions generally require some numerical methods. Here, a finite-difference method was used.[24,25] To carry out the discretization, the implicit backward difference and central difference schemes were applied. The discretized equations of micropore and macropore mass balances are both tridiagonal systems, which can be easily solved by the Gauss elimination method. Assuming that all the variables (namely $A_{\mu_i}^n$ and A_j^n, where the subscripts i, j and n refer to the spatials of micropore, macropore and time variables, respectively) are known, the values of $A_{\mu_i}^{n+1}$ and A_j^{n+1} can be found iteratively, and then the procedure is repeated until the desired degree of convergence is achieved. The finite-difference implicit method is given in the Appendix. To solve the equations, a program written in FORTRAN was developed. Using the scheme of Gauss elimination with main element chosen and finite-difference implicit method adopted, the solving procedure was stable. The numerical computation was performed using AMD K6-2 400MHZ computer, and the average CPU time was about 30–60 s.

Experimental System

The adsorption equilibrium capacity and the adsorption kinetics of sulfur dioxide onto the activated carbon prepared from the agricultural byproduct, pistachio-nut shell, were determined by a thermogravimetric analysis system, which is shown in Figure 1. The preparation of the activated carbon from pistachio-nut shell was reported elsewhere by the authors.[26] SO_2 gas in various concentrations (1,000 ppm, 2,000 ppm, 3,000 ppm and 4,000 ppm with nitrogen as the carrier gas and supplied by Singapore Oxygen Air Liquide Pte, Ltd.) was introduced into the analyzer chamber where a platinum sample holder with about 10 mg of activated

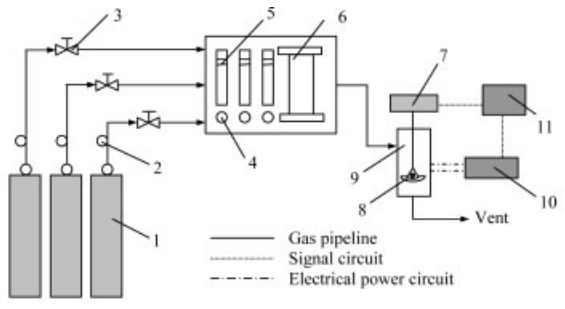

1. Gas cylinder 2. Pressure gauge 3. Regulating valve 4. Fine adjustable valve
5. Rotameter 6. Mixing chamber 7. Microbalance 8. Sample holder
9. Heating furnace 10. Control panel 11. Computer

Figure 1. Experimental setup.

Table 2. Physical Properties of Activated Carbon Prepared from Pistachio-nut shell

True density	2.05 g/cm^3
Apparent density	1.01 g/cm^3
Total porosity	0.51
Micropore porosity	0.16
Macropore porosity	0.35
Radius of particle	0.75 mm
Radius of microsphere	1.325×10^{-9} m
Average macropore diameter	3.36×10^{-8} m
BET(N_2) surface area	1064 m^2/g

carbons was suspended. At the beginning of the experiment, the carbon samples were dried by heating up to 350°C at a heating rate of 10°C/min, and held for 30 min before cooling down to the temperature required for the adsorption test. All these temperature programs were controlled by the temperature controller which was connected to a personal computer. After regeneration of the activated carbon, the sorbate gas mixture was introduced to the gas chamber. At a certain temperature, the sample weight gain due to the amount of SO_2 adsorbed was recorded until no further weight change was observed. Tests were conducted at different temperatures ranging from 25 to 100°C to study the temperature effect on adsorption. The properties of the activated carbon are given in Table 2.

Results and Discussion

(a) Theoretical analysis

Sorbent Equilibrium Capacity. The experimentally determined equilibrium adsorption capacity of sulfur dioxide onto the activated carbon at 25°C for different SO_2 concentrations and the different types of isotherms are shown in Figure 2. The values of the constants for each isotherm are listed in Table 3 (The isotherm expressions are given in Table 1). For the two-parameter isotherms (Freundlich and Langmuir), the isotherms were determined using the least squares regression method while for the three-parameter isotherms (Sips, Toth and R-P), the least-squares method was combined with the simplex method, the latter being used for searching the exponent n. As could be seen from Figure 2 and Table 3, each isotherm relationship fits the data quite well and has a similar average error, apart from the slightly higher deviation for the Freundlich isotherm.

Effect of isotherm type on kinetic model

Before the model simulations were used to fit the experimental data, the validity of using each isotherm in the computer model was examined. As shown in Figure 2, the experimentally determined equilibrium adsorption capacity data

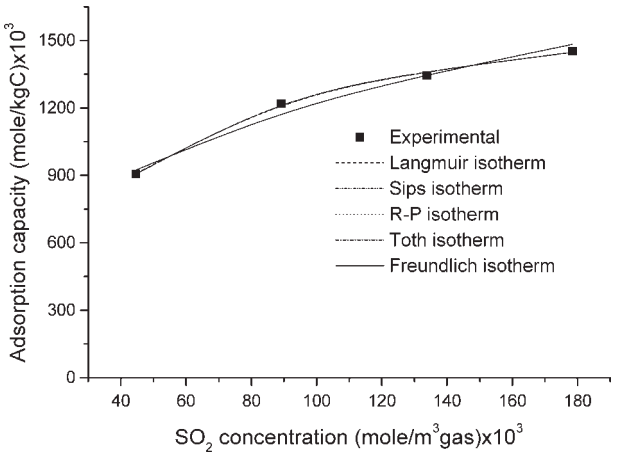

Figure 2. Sulfur dioxide adsorption isotherms on activated carbon at 25°C.

agreed reasonably well with each of the five different types of isotherms. However, it was not known whether all the isotherm equations would produce similar numerical adsorption or desorption dynamic simulations. The suitability of the five isotherm types was determined by carrying out numerical kinetic simulations using a concentration-dependent surface diffusivity micropore, surface and macropore diffusion (CDSDMSMD) control model. These kinetic adsorption and desorption simulations using the five isotherms are shown in Figure 3a and b, respectively.

Figure 3 shows that the adsorption and desorption kinetic curves using each of the five different isotherms agree very well with each other, apart from some very slight differences which are probably due to the five isotherms having different gradients for the same adsorbate concentration. Hence, in the numerical simulations, the five different isotherms can be used in the sorption kinetic calculation. However, there are restrictions imposed on the Freundlich isotherm, which cannot be used when the HIO or Do model is used in the simulations.

The results in Figure 3a and b show that the different types of nonlinear isotherms used in the kinetic model have little effect on the overall particle uptake kinetics. Hence, the Langmuir equation was chosen for the kinetic model in this study because of its flexibility in the use of the kinetics parameters and the least computing time required.

After fixing the isotherm type (Langmuir isotherm), the experimental determined equilibrium capacities of sulfur dioxide onto the activated carbons at different temperatures were again fitted to the Langmuir isotherm as shown in Figure 4.

Figure 4 shows that the Langmuir isotherm matches the experimental data very well over a range of concentrations

Table 3. Values of Isotherm Constants at 25°C

Isotherm	q_m (mole/kgC)	b (m^{3}gas/mole)	n	K (m^{3}gas/kgC)	Ave. error (%)
Langmuir	1.806	22.68			0.62
Sips	1.779	25.92	1.035		0.57
Fruendlich			2.935	2.667	2.01
R-P	1.766	22.37	1.018		0.58
Toth	1.774	25.64	1.052		0.57

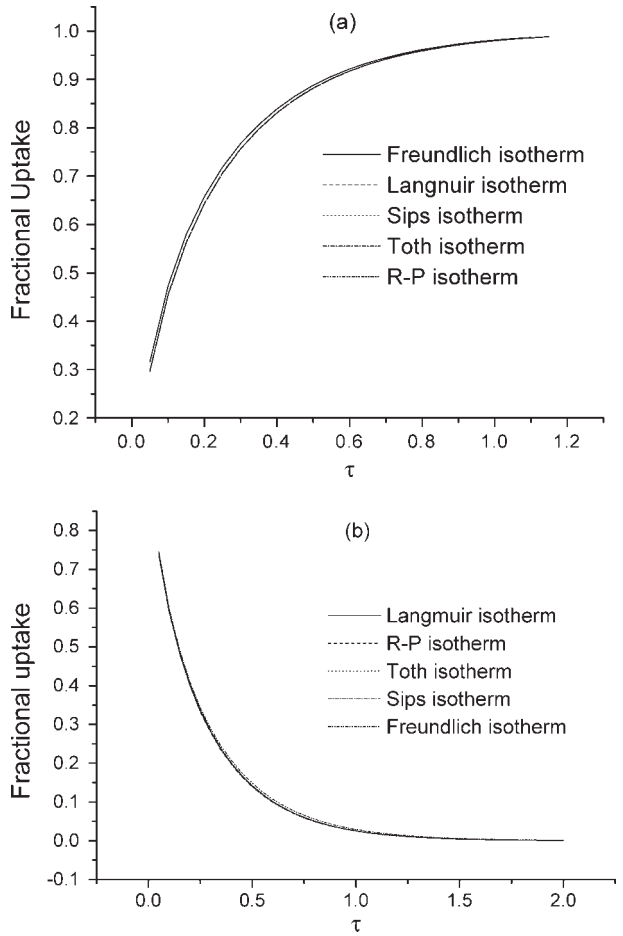

Figure 3. Effects of isotherm type on (a) adsorption kinetics, and (b) desorption kinetics.

Model parameters: $\gamma = 0.41$, $\delta = 0.68$, $Bi_m = 97$, $\sigma_1 = 0.01$, $\sigma_2 = 0.99$, $S = 2$.

and temperatures. The extracted values of b, while keeping q_m (Eq. 1b) constant, were obtained as shown in Table 4. The heat of adsorption, $-\Delta H$, was determined by fitting the

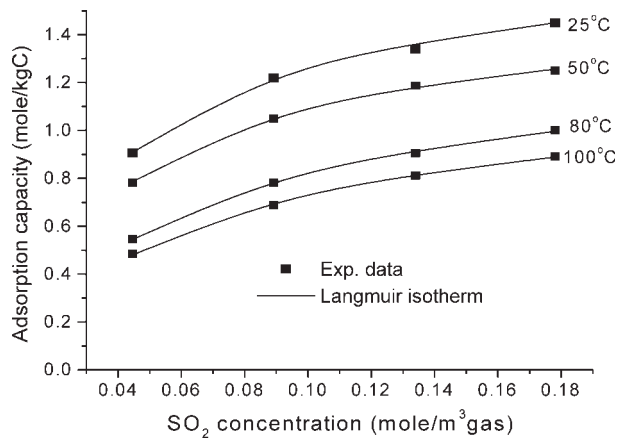

Figure 4. SO_2 adsorption isotherms on activated carbon at different temperatures.

Table 4. Values of Langmuir Isotherm Constants at Various Temperatures

Temp.(°C)	b (m^3gas/mole)	q_m (mole/kgC)
25	22.68	1.805
50	14.72	1.805
80	8.068	1.805
100	6.52	1.805

Langmuir isotherm equilibrium constant (b) to the van't Hoff equation

$$b = b_0 \exp\left(\frac{-\Delta H}{RT}\right) \tag{19}$$

Using Eq. 19, the heat of adsorption of SO_2, $-\Delta H$, was calculated to be 15.8 kJ/mole. This value was similar to that estimated by Wakao and Kaguei,[27] which was 15 kJ/mole. This value was also of the same order of magnitude but smaller than that ($-\Delta H$) value of 22.6 kJ/mole (for Norit RB commercial activated carbon) obtained by Gray and Do.[13] The reason could be due to the different physical and chemical properties of the various adsorbents.

Effect of concentration-dependent surface diffusivity on the kinetics model

The effect of the concentration-dependent surface diffusivity on the overall uptake was studied by comparing the results for the concentration-dependent surface diffusivity micropore, surface and macropore diffusion (CDSDMSMD) control model, and the constant surface diffusivity micropore, surface and macropore diffusion (CSDMSMD) control model. The two models were used and compared for the adsorption of sulfur dioxide onto the activated carbon. The results are shown in Figure 5. It can be seen that the effect of using the concentration-dependent surface diffusivity (HIO or Do model) is to increase the overall uptake. Due to concentration dependence, the surface diffusivity value and the resulting flux at the particle surface in the CDSDMSMD

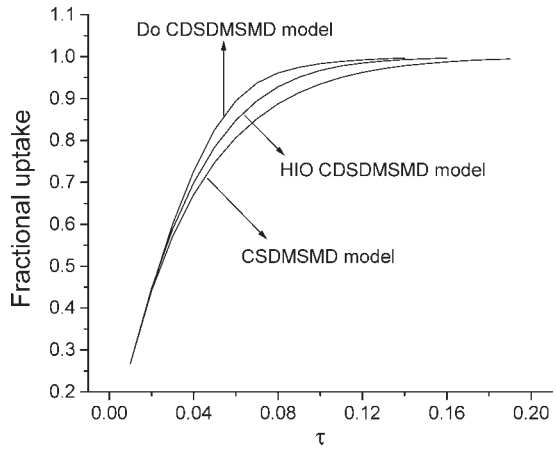

Figure 5. Effect of surface diffusivity type on adsorption kinetics.

Model parameters: $\gamma = 5$, $\delta = 2$, $Bi_m = 97$, $\sigma_1 = 0.089$, $\sigma_2 = 0.911$, $S = 2$, $\lambda = 2.5$.

model are higher than those used in the CSDMSMD model. Therefore, the overall uptake given by the CDSDMSMD model is higher than that for the CSDMSMD model at any given time. At the same time, there is a stronger concentration-dependence in the Do model than in the HIO model, so the overall uptake given by the Do CDSDMSMD model is higher than that for the HIO CDSDMSMD model at any given time.

Particle concentration profiles

Model simulations can be used to gain an insight into the processes occurring inside the carbon sorbent particle, namely by observing the changes in concentration profiles within the macropore and micropore of the adsorbent. Figures 6a–c show the model simulation concentration profiles. The macropore concentration profile in Figure 6a shows a significant steep gradient, especially in small uptakes. The concentration at the surface ($x = 1$) is not equal to the bulk concentration (i.e., $A \neq 1$) due to the existence of some external mass transfer resistance (i.e., the mass transfer Biot number is not large enough). Figure 6b and c show the corresponding micropore profiles at uptakes of 0.25 and 0.70, respectively. With increasing uptake, the micropore concentration gradient decreases due to the diffusion of the adsorbate into the center of the micropore particle.

(b) Comparison between experimental results and model simulations

Determination of D/R_μ^2, D_p and D_s. The experimental adsorption kinetic data for the activated carbon prepared from the pistachio-nut shell were fitted using the concentration-dependent surface diffusivity micropore, surface, macropore diffusion (CDSDMSMD) control model to determine the parameters D/R_μ^2,D_p and D_s. The model was initially fitted to two groups of data for adsorption of SO_2 on a 0.75 mm spherical particle. One was the adsorption data for the concentration range of 1,000 to 4,000 ppm at 25°C, and the other was the adsorption data for temperature range 25 to 100°C at 1,000 ppm. The mass transfer Biot number (Bi_m) used in the model was calculated from the Ranz-Marshall correlation for single particles[27]

$$Bi_m = \frac{D_a}{2D_p\varepsilon_m}\left(2 + 1.1Sc^{1/3}\mathrm{Re}^{0.6}\right) \tag{20}$$

During the fitting procedures, three diffusivities were used as the fitting parameters. However, there is a certain relationship between the macropore diffusivity D_p, and the variation in temperature. Since the macropore diffusion consists of Knudsen and molecular diffusion which are both linked to temperature (details are given in the next section, see Eqs. 22–24), therefore, the correlation of $D_p \propto T^\alpha$ is reasonable.

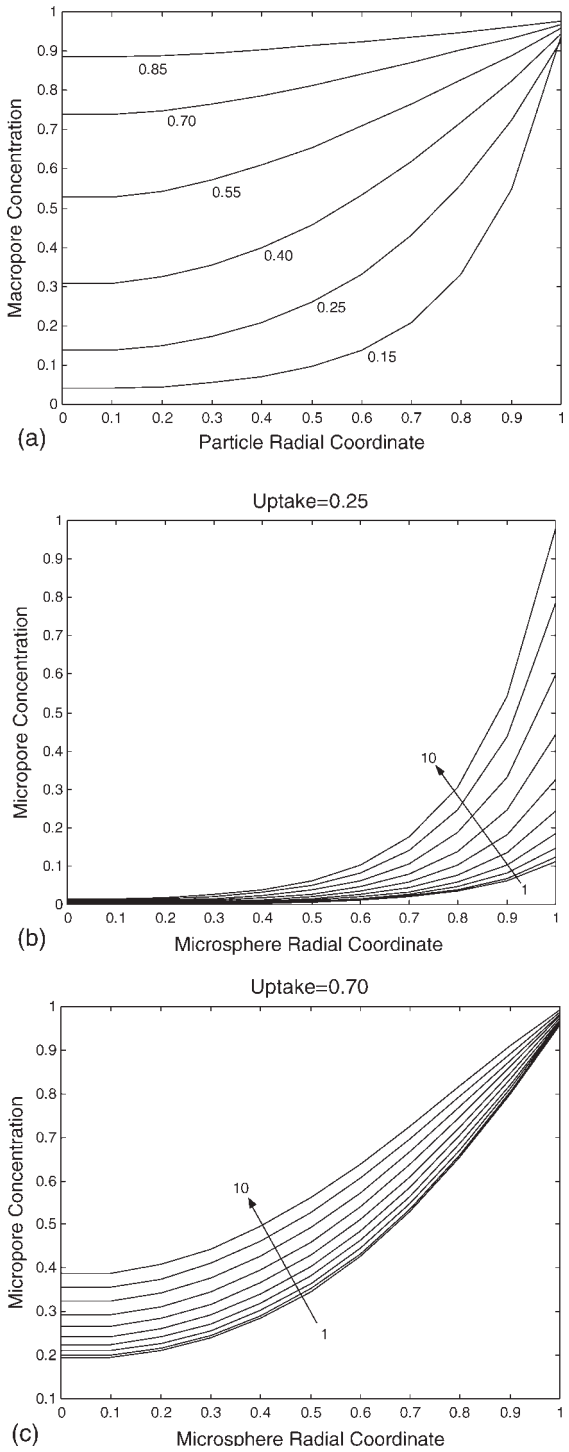

Figure 6. (a) Macropore concentration profile (the number on each curve refers to the particle uptake). Model parameters: $\gamma = 2$, $\delta = 3$, $Bi_m = 97$, $\sigma_1 = 0.01$, $\sigma_2 = 0.99$, $\lambda = 2$, S = 2, HIO model, (b) micropore concentration profile at uptake 0.25 (each curve refers to the macropore grid point on which each micropore profile is calculated, ranging from 1 near the center to 10 near the surface of the particle). Model parameters: $\gamma = 2$, $\delta = 3$, $Bi_m = 97$, $\sigma_1 = 0.01$, $\sigma_2 = 0.99$, $\lambda = 2$, S = 2, HIO model, and (c) micropore concentration profile at uptake 0.70 (each curve refers to the macropore grid point on which where each micropore profile is calculated, ranging from 1 near the center to 10 near the surface of the particle). Model parameters: $\gamma = 2$, $\delta = 3$, $Bi_m = 97$, $\sigma_1 = 0.01$, $\sigma_2 = 0.99$, $\lambda = 2$, S = 2, HIO model.

Table 5. SO_2 Macropore, Surface and Micropore Diffusivities from Model Fitting to 0.75 mm Spherical Particle Adsorption Data at Various Temperatures and SO_2 Concentrations

Temperature (°C)	D_p (m^2/s)	D/R_μ^2 (s^{-1})	D_s (m^2/s)
25	3.815×10^{-7}	8.175×10^{-5}	1.288×10^{-11}
50	4.09×10^{-7}	9.36×10^{-5}	1.488×10^{-11}
80	4.413×10^{-7}	1.128×10^{-4}	1.939×10^{-11}
100	4.618×10^{-7}	1.26×10^{-4}	2.085×10^{-11}

Using the data obtained in the experimental conditions, it was found that $\alpha = 0.85$. The values of D/R_μ^2, D_p and D_s extracted from the curve fitting were found and the average values as given in Table 5 were used.

In chemical engineering, the Arrhenius expression is used to explain the temperature effect on the reaction rate. This expression is given as

$$K_r = K_{r0} e^{-E/RT} \tag{21}$$

Thus, the values of D/R_μ^2 and D_s extracted at each temperature were fitted to the Arrhenius expression to give the activation energy for micropore diffusivity $E_\mu = 5.363$ kJ/mole, and for surface diffusivity $E_s = 6.245$ kJ/mole. These two values were of the expected order of magnitude, and quite close to the results obtained by other researchers.[12,13]

The experimental results with the fitted simulation curves using the extracted diffusivities in Table 5 are shown in Figures 7 and 8. In Figure 7, the simulation results using the HIO and Do models are quite close to each other and indistinguishable over most of the time scale when the adsorbate bulk concentrations used are low, such as 1,000 ppm and 2,000 ppm. However, when the adsorption kinetic tests were carried out at higher concentrations, such as 3,000 and 4,000 ppm, differences had surfaced between the HIO model and Do model results. In Figure 7, it can be seen that for low concentrations (1,000 and 2,000 ppm), the curves from

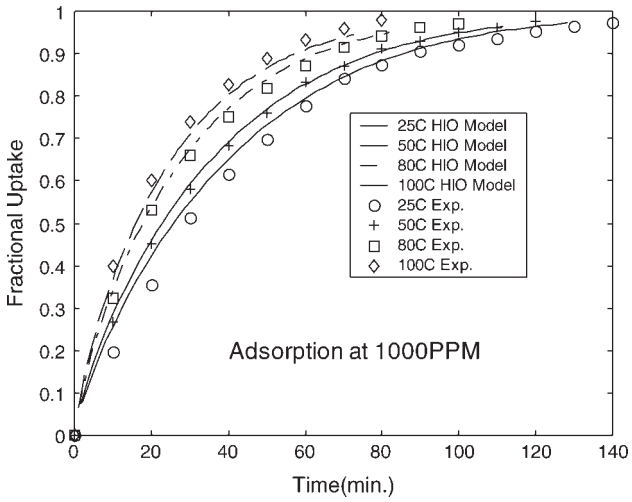

Figure 8. Comparison between model fitting curves and SO_2 experimental adsorption data: Effect of temperature at fixed concentration of 1,000 ppm.

both the Do and HIO models collapse together and superimpose with each other. These curves match the experimental data well, while for higher concentrations of 3,000 and 4,000 ppm, the Do model shows better agreement with the experimental results than the HIO model although small deviations still exist. Figure 8 shows the effect of temperature on the fractional uptake for a concentration of 1000 ppm. The HIO model simulation curves agree with the experimental data fairly closely over a wide range of temperatures.

Figure 7 shows that the uptake curves become slower when the gas concentration decreases. This is because as the SO_2 concentration decreases, the ratio q_0/C_0 increases (due to the favorable nature of the isotherm), hence, γ also increased (Eq. 9). Therefore, the resultant increase in macropore resistance renders the adsorption uptake slower.

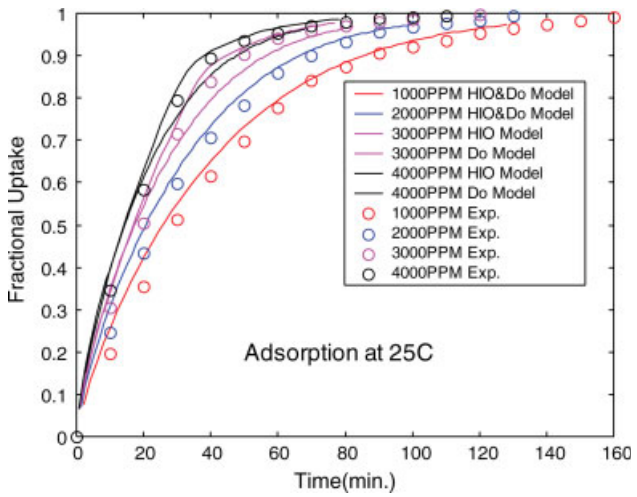

Figure 7. Comparison between model fitting curves and SO_2 experimental adsorption data: Effect of concentration at fixed temperature of 25°C.

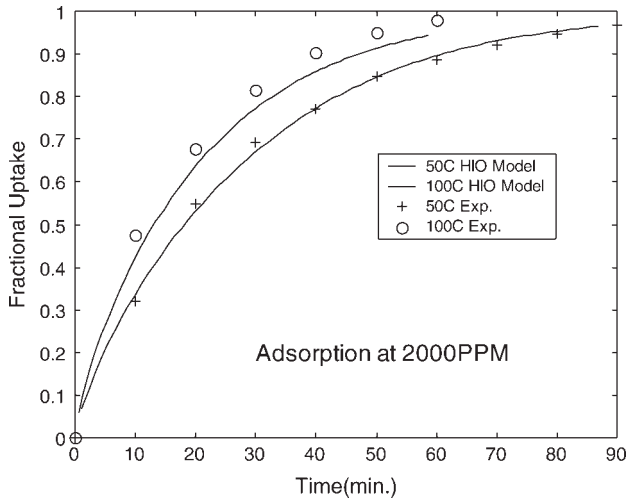

Figure 9. Comparison between model prediction of adsorption kinetics curves and experimental data with different temperatures at concentration of 2,000 ppm.

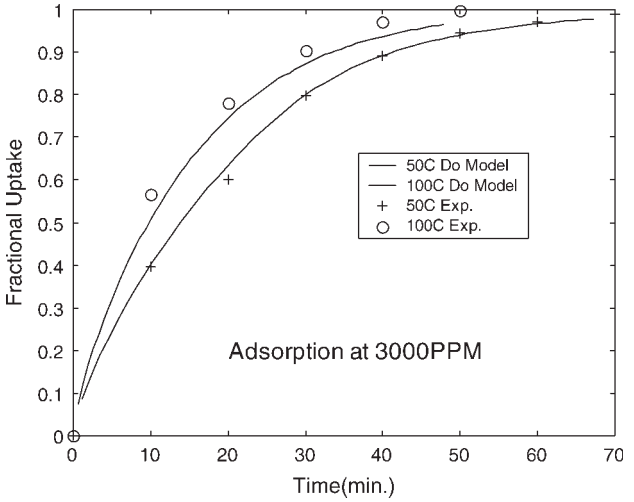

Figure 10. Comparison between model prediction of adsorption kinetics curves and experimental data with different temperatures at concentration of 3,000 ppm.

To further test the validity of the CDSDMSMD model, the model together with the extracted diffusivities was used to predict the fractional uptake curves at other temperatures and concentration conditions which were different from those used for the initial fitting to determine the diffusivity parameters. These experimental data together with the model simulations are shown in Figures 9 and 10.

Figures 9 and 10 show the adsorption kinetic curves for SO_2 adsorption for 2,000 and 3,000 ppm, respectively, at various temperatures. It can be seen that the model agrees well with the experimental data, apart from the slight deviation for the higher-temperature data at 100°C.

Figures 8, 9 and 10 show that when the adsorption temperature increases, the uptake rate also increases. This is physically expected because increased temperature results in increased diffusivities for the micropore, macropore and surface diffusions. Thus, faster uptake curves are obtained.

In adsorption modeling, it is possible that many models can often provide good agreement with the transient uptake data. However, the validity of a proposed model is best established either by comparison of the fitted parameters with independent estimates, or by determining if the variation of the fitted parameters with experimental conditions is consistent with the physical assumptions in which the model is based. So, in this case, the extracted value of the macropore diffusivity D_p from the model developed in this study was used to calculate the tortuosity factor τ, and then this τ value was used to verify the validity of the model by comparing with experimental or other known values.

Determination of tortuosity factor

Diffusion in the gas phase results from collisions. Collisions among the gas molecules dominate the process for diffusion in a large pore and thus this diffusion is the same as bulk diffusion, referred to as molecular diffusion. When the pore diameter becomes smaller, collisions between the molecules and the pore wall become increasingly important. In a very small pore, collisions with the pore wall dominate, and the diffusion process assumes an entirely different mechanism, known as Knudsen diffusion. The relative importance of the two different mechanisms for diffusion is determined by the ratio of the pore diameter to the mean free path of the gas molecules. Normally, molecular diffusion prevails when the pore diameter is greater than 10 times the mean free path; Knudsen diffusion may be assumed when the mean free path is greater than 10 times the pore diameter.

In the Knudsen diffusion regime, the diffusivity is given by Kauzmann[28]

$$D_k = 97.0\bar{r}\left(\frac{T}{M}\right)^{1/2} \tag{22}$$

The molecular diffusivity for a binary gas mixture at low-pressure is inversely proportional to the pressure, increases with increasing temperature and is almost independent of the composition for a given gas-pair. The following equation for the estimation of D_m at low pressure has been developed from a combination of kinetic theory and corresponding states arguments[29]

$$\frac{pD_m}{(p_{cA}p_{cB})^{1/3}(T_{cA}T_{cB})^{5/12}(\frac{1}{M_A}+\frac{1}{M_B})^{1/2}} = a\left(\frac{T}{\sqrt{T_{cA}T_{cB}}}\right)^b \tag{23}$$

Both the molecular and Knudsen diffusions may be operative simultaneously. For the self-diffusion or equimolar counter transfer, the gas-phase diffusivity can be written as

$$\frac{1}{D_g} = \frac{1}{D_m} + \frac{1}{D_k} \tag{24}$$

The aforementioned equation (Eq. 22) gives the diffusivity in a single cylindrical pore. The pores in the highly porous material, such as activated carbon, however, are interconnected void spaces. So in order to account for the tortuous path of the molecule rather than along the radial direction and the porosity of the adsorbent for the fact that diffusion occurs only in the pore space, the effective diffusivity is used

$$D_e = \frac{\varepsilon}{\tau}D_g \tag{25}$$

Tortuosity is essentially a geometric factor which is independent of either temperature or the nature of the diffusion species. Experimental tortuosity factors generally fall within the range of 2–6.[8]

Based on the adsorption results for the activated carbon from pistachio-nut shell at 25°C and other experimental conditions, the following values were obtained: $\varepsilon = 0.51$, $D_m = 1.26\cdot10^{-5}\text{m}^2/\text{s}$, $D_k = 5.31\cdot10^{-6}\text{m}^2/\text{s}$ and D_e = the extracted D_p ($=3.815\cdot10^{-7}\text{m}^2/\text{s}$). Therefore, a tortuosity τ of 5 was obtained. This value agreed with the values given by Costa et al.[21] on activated carbons, for τ ranging from 4 to 6.

A simple equation adequate only for an approximate estimation of τ is given by Mackie and Meares[30] such that

$$\tau = \frac{(2-\varepsilon)^2}{\varepsilon} \tag{26}$$

For a porosity of 0.51, Eq. 26 gives a τ value of 4.35, which is of the same order of magnitude as the value of 5 determined in this study. Hence, the value of τ obtained verifies the validity of the CDSDMSMD model used in this study.

Conclusions

The adsorption study of SO_2 onto activated carbon prepared from pistachio-nut shell was studied theoretically and experimentally. CDSDMSMD model of adsorption kinetics incorporating micropore, macropore and surface diffusion, together with a nonlinear isotherm at the micropore mouth has been derived and solved by finite difference method. The effects of different types of nonlinear isotherms and concentration dependent surface diffusivities have been thoroughly studied. The simulation results show that different types of nonlinear isotherms used in the kinetic model have little effect on the overall particle uptake kinetics. The different surface diffusivity models such as constant surface diffusivity, HIO model surface diffusivity, and Do model surface diffusivity will have some effects on the adsorption kinetics, especially when the bulk concentration is high. The effects of concentration and temperature were studied experimentally. Good agreement was found between the model predictions and the experimental results. The value of the tortuosity factor and the extracted diffusion coefficients are consistent with published values in the literature, confirming the validity of the theoretical model.

Notation

A = dimensionless macropore concentration
A_b = dimensionless bulk-gas concentration
A_μ = dimensionless microsphere concentration
$\overline{A}_\mu$ = dimensionless average microsphere concentration
b, n, K = constants in isotherms
b_0 = the nature of a frequency factor
Bi_m = mass transfer Biot number
C = the adsorbate concentration in the macropore
C_0 = the initial adsorbate concentration in the macropore
C_b = the adsorbate concentration in the bulk-gas phase
D = the micropore diffusivity
Da = molecular diffusivity of adsorbate in bulk air
D_e = effective diffusivity
D_g = gas-phase diffusivity
D_k = the Knudsen diffusivity
D_m = molecular diffusivity between A and B
D_p = the macropore diffusivity
D_s = the surface diffusivity
D_{s0} = D_s at zero coverage
d = diameter of adsorbent particle
E = activation energy
K_m = the external film mass transfer coefficient
K_r = reaction rate
K_{r0} = constant
M = molecular weight
M_A and M_B = molecular weights for gases A and B, respectively
p = total pressure
p_{cA}, p_{cB} = critical pressures for gases A and B, respectively
q = the adsorbate concentration in the microsphere
$\overline{q}$ = the volume average microsphere concentration
q_0 = the initial adsorbate concentration in the micropore
q_m = maximum sorbed phase concentration in the Langmuir isotherm
R = the particle radius, or gas constant, 8.314 J/mole/K
Re = Reynolds number, vd/ν
R_μ = the microsphere radius
r = the particle radial coordinate
r_μ = the microsphere radial coordinate
$\overline{r}$ = the average pore radius of the adsorbent
s = the particle shape factors, s = 0,1,2 for slab, cylinder and sphere, respectively
Sc = Schmidt number, ν/Da
T = temperature of adsorption
t = real-time coordinate
T_{cA},T_{cB} = critical temperatures for gases A and B, respectively
v = fluid velocity in the thermogravimetric analyzer chamber
x = dimensionless particle radial coordinate
x_μ = dimensionless microsphere radial coordinate
γ = ratio of macropore to micropore diffusional resistances
$-\Delta H$ = the heat of adsorption
δ = ratio of surface to macropore diffusional fluxes
ε = porosity of the adsorbent
ε_m = macropore porosity
θ = surface coverage
λ = measure of the isotherm nonlinearity
ν = kinematic viscosity of air
σ_1 = dimensionless macropore capacity
σ_2 = dimensionless microsphere capacity
τ = dimensionless time, or tortuosity

Literature Cited

1. Lin TF, Little JC, Nazaroff WW. Transport and sorption of volatile organic component compounds and water vapor within dry soil grains. *Environ Sci Technol*. 1994;28:322–330.
2. Lin TF, Little JC, Nazaroff WW. Transport and sorption of organic gases in activated carbon. *J Environ Eng-ASCE*. 1996;122:169–175.
3. Ganguly SK, Goswami AN. Surface diffusion kinetics in the adsorption of acetic acid on activated carbon. *Sep Sci Technol*. 1996;31:1267–1278.
4. Chatzopoulos D, Varma A, Irvine RL. Activated carbon adsorption and desorption of toluene in the aqueous phase. *AIChE J*. 1993;39:2027–2041.
5. Lin TF, Nazaroff WW. Transport and sorption of water vapor in activated carbon. *J Environ Eng-ASCE*. 1996;122:176–182.
6. Furuya EG, Chang HT, Miura Y, Yokomura H, Tajima S, Yamashita S, Noll KE. Intraparticle mass transport mechanism in activated carbon adsorption of phenols. *J Environ Eng-ASCE*. 1996;122:909–916.
7. Do DD. Adsorption in porous solids having bimodal pore size distribution. *Chem Eng Commun*. 1983;23:27–56.
8. Ruthven DM. *Principles of Adsorption and Adsorption Processes*. New York: John Wiley & Sons; 1984.
9. Gray PG, Do DD. Adsorption and desorption of gaseous sorbates on a bidispersed particle with Freundlich isotherm. I. Theoretical analysis. *Gas Sep Purif*. 1989;3:193–200.
10. Gray PG, Do DD. Adsorption and desorption of gaseous sorbates on a bidispersed particle with Freundlich Isotherm. II. Experimental study of sulfur dioxide sorption on activated carbon particles. *Gas Sep Purif*. 1989;3:201–208.
11. Yang RT. *Gas Separation by Adsorption Processes*. Boston: Butterworths, 1987.
12. Kapoor A, Yang RT, Wong C. Surface diffusion. *Catal Rev-Sci Eng*. 1989;31:129–214.
13. Gray PG, Do DD. Adsorption and desorption of gaseous sorbates on a bidispersed particle with Freundlich isotherm. III. Contribution of surface diffusion to the sorption dynamics of sulfur dioxide on activated carbon. *Gas Sep Purif*. 1990;4:149–157.
14. Gray PG, and Do DD. Dynamics of carbon dioxide sorption on activated carbon particles. *AIChE J*. 1991;37:1027–1034.
15. Higashi K, Ito H, Oishi J. Surface diffusion phenomena in gaseous diffusion. I. Surface diffusion of pure gas. *J At Energy Soc Jpn*. 1963;5:846–853.
16. Gray PG. A fundamental study on removal of air pollutants (sulfur dioxide, nitrogen dioxide and carbon dioxide) by adsorption on activated carbon. *Gas Sep Purif*. 1993;7:213–224.
17. Grzegorczyk DS, Carta G. Adsorption of amino acids on porous polymeric adsorbents - II. Intraparticle mass transfer. *Chem Eng Sci*. 1996;51:819–826.
18. Calleja G, Serna J, Rodriguez J. Kinetics of adsorption of phenolic compounds from wastewater onto activated carbon. *Carbon*. 1993;31:691–697.
19. Seidel A, Carl PS. The concentration dependence of surface diffusion for adsorption on energetically heterogeneous adsorbents. *Chem Eng Sci*. 1989;44:189–194.
20. Bhatia SK. Combined surface and pore volume diffusion in porous media. *AIChE J*. 1988;34:1094–1105.

21. Costa E, Calleja G, Domingo F. Adsorption of gaseous hydrocarbons on activated carbon: Characteristic kinetic curve. *AIChE J*. 1985;31:982–991.
22. Kapoor A, Yang RT. Contribution of concentration-dependent surface diffusion to rate of adsorption. *Chem Eng Sci*. 1991;46:1995–2002.
23. Do DD. A model for surface diffusion of ethane and propane in activated carbon. *Chem Eng Sci*. 1996;51:4145–4158.
24. Lapidus L, Pinder GF. *Numerical Solution of Partial Differential Equations in Science and Engineering*. New York: John Wiley & Sons; 1982.
25. Tien C. *Adsorption Calculations and Modeling*. Boston: Butterworth-Heinemann; 1994.
26. Yang T, Lua AC. Characteristics of activated carbons prepared from pistachio-nut shells by physical activation. *J. Colloid Interface Sci*. 2003;267:408–417.
27. Wakao N, Kaguei S. *Heat and Mass Transfer in Packed Beds*. New York: Gordon and Breach; 1982.
28. Kauzmann W. *Kinetic Theory of Gases*. New York: Benjamin; 1966.
29. Bird RB, Stewart WE, Lightfoot EN. *Transport Phenomena*. New York: John Wiley & Sons; 1960.
30. Mackie JS, Meares P. The diffusion of electrolytes in a cation-exchange resin membrane. I. Theoretical. *Proc R Soc A-Math Phys Sci*. 1955;232:498.

Appendix

The equations in the single-particle sorption model can be solved using the finite-difference implicit method. The time and spatial derivatives are approximated as follows

$$\left(\frac{\partial A_\mu}{\partial \tau}\right)_{i,n+1} = \frac{A_{\mu_{i,n+1}} - A_{\mu_{i,n}}}{\Delta\tau} \tag{A1}$$

$$\left(\frac{\partial A_\mu}{\partial x_\mu}\right)_{i,n} = \frac{A_{\mu_{i+1,n}} - A_{\mu_{i-1,n}}}{2\Delta x_\mu} \tag{A2}$$

$$\left(\frac{\partial^2 A_\mu}{\partial x_\mu^2}\right)_{i,n} = \frac{A_{\mu_{i+1,n}} - 2A_{\mu_{i,n}} + A_{\mu_{i-1,n}}}{\Delta x_\mu^2} \tag{A3}$$

where the subscripts i and n refer to the spatial of micropore and time variables, respectively (the derivatives of A are similar to those of A_μ). Assuming that a micropore is divided into N intervals with N+1 grid points (with $i = 1$ at $x_\mu = 0$, and $i = N+1$ at $x_\mu = 1$), and substituting Eqs. A1, A2, and A3 into Eqs. 14, 14a,b, and 16a, the following discretised equations for microsphere can be obtained

$$A_{\mu_i}^{n+1}\left(\frac{{x_{\mu_i}}^2\Delta x}{\Delta\tau} + \frac{\gamma {x_{\mu_{i+1/2}}}^2}{\Delta x} + \frac{\gamma {x_{\mu_{i-1/2}}}^2}{\Delta x}\right) = A_{\mu_{i+1}}^{n+1}\frac{\gamma {x_{\mu_{i+1/2}}}^2}{\Delta x} + A_{\mu_{i-1}}^{n+1}\frac{\gamma {x_{\mu_{i-1/2}}}^2}{\Delta x} + A_{\mu_i}^{n}\frac{{x_{\mu i}}^2\Delta x}{\Delta\tau} \quad 2 \le i \le N \tag{A4}$$

$$A_{\mu_i}^{n+1} = A_{\mu_{i+1}}^{n+1} \quad i = 1 \tag{A5}$$

$$A_{\mu_i}^{n+1} = \frac{(1+\lambda)A_j^{n+1}}{(1+\lambda A_j^{n+1})} \quad \text{(for Langmuir isotherm)} \quad i = N+1;\ \ j = 1, N+1 \tag{A6}$$

$$A_{\mu_i}^{1} = A_j^1 = 0 \quad i = 1, N+1;\ \ j = 1, N+1 \tag{A7}$$

where

$$x_{\mu_i} = (i-1)\Delta x_\mu \quad x_{\mu_{i+1/2}} = \left(i - \frac{1}{2}\right)\Delta x_\mu \quad x_{\mu_{i-1/2}} = \left(i - \frac{3}{2}\right)\Delta x_\mu \tag{A8}$$

j refers to the spatial of macropore variables.

Similiarly, the following discretized equations for the macropore can be obtained.

$$A_j^{n+1}\left(\frac{\sigma_1 x_j^2}{\Delta\tau} + \frac{x_{j+1/2}^2}{\Delta x^2} + \frac{x_{j-1/2}^2}{\Delta x^2}\right) = A_{j+1}^{n+1}\left(\frac{x_{j+1/2}^2}{\Delta x^2}\right) + A_{j-1}^{n+1}\left(\frac{x_{j-1/2}^2}{\Delta x^2}\right) + \delta\bar{A}_{\mu x_j}^{n+1}(1+\lambda A_j^n) + \frac{\sigma_1 x_j^2}{\Delta\tau}A_j^n - \sigma_2\bar{A}_{\mu_{t,j}}^{n+1}x_j^2 \quad \text{(for HIO model)} \quad 2 \le j \le N \tag{A9}$$

$$A_j^{n+1} = A_{j+1}^{n+1} \qquad \bar{A}_{\mu_j}^{n+1} = \bar{A}_{\mu_{j+1}}^{n+1} \qquad j = 1 \tag{A10}$$

$$A_j^{n+1}(1 + Bi_m\Delta x) - A_{j-1}^{n+1} = Bi_m\Delta x A_b - \delta\left(\bar{A}_j^{n+1} - \bar{A}_{j-1}^{n+1}\right)(1+\lambda A_j^n) \quad j = N+1 \tag{A11}$$

where

$$\bar{A}_{\mu_{ij}}^{n+1} = \frac{\bar{A}_{\mu_j}^{n+1} - \bar{A}_{\mu_j}^{n}}{\Delta\tau} \quad j = 1, N+1 \tag{A12}$$

$$\bar{A}_{\mu_{x,j}}^{n+1} = \frac{x_{i+1/2}^2\left(\bar{A}_{\mu_{j+1}}^{n+1} - \bar{A}_{\mu_j}^{n+1}\right) - x_{i-1/2}^2\left(\bar{A}_{\mu_j}^{n+1} - \bar{A}_{\mu_{j-1}}^{n+1}\right)}{\Delta x^2} \quad j = 1, N+1 \tag{A13}$$

$$x_i = (i-1)\Delta x \quad x_{i+1/2} = \left(i - \frac{1}{2}\right)\Delta x \quad x_{i-1/2} = \left(i - \frac{3}{2}\right)\Delta x \tag{A14}$$

$\bar{A}_\mu = 3\int_0^1 x_\mu^2 A_\mu dx_\mu$, and this integration can be carried out numerically using Simpson's rule, one of the compound quadrature formulae.

The discretized equations of micropore and macropore are both tridiagonal systems which can be easily solved by Gauss elimination method. Assuming that all the variables (namely $A_{\mu_i}^n$ and A_j^n $i = 1, N+1$; $j = 1, N+1$) are known, the values of $A_{\mu_i}^{n+1}$ and A_j^{n+1} can be found using Eqs. A4–A14 iteratively, and then the procedure is repeated until the desired degree of convergence is achieved.

To solve the aforementioned equations, a program written in FORTRAN was developed. The convergence criteria were: $\left|\frac{A_{\mu_i}^{n+1} - A_{\mu_i}^n}{A_{\mu_i}^n}\right| \le 10^{-3}$ and $\left|\frac{A_j^{n+1} - A_j^n}{A_j^n}\right| \le 10^{-3}$.

Manuscript received Nov. 12, 2007, and revision received Aug. 28, 2008.